JACS
JOURNAL OF THE AMERICAN CHEMICAL SOCIETY
Article
pubs.acs.org/JACS

Dithieno[3,2-*c*:2′,3′-*e*]-2,7-diketophosphepin: A Unique Building Block for Multifunctional π-Conjugated Materials

Xiaoming He, Javier Borau-Garcia, Alva Y. Y. Woo, Simon Trudel, and Thomas Baumgartner*

Department of Chemistry and Centre for Advanced Solar Materials, University of Calgary, 2500 University Drive NW, Calgary, Alberta, Canada T2N 1N4

Supporting Information

ABSTRACT: A series of conjugated materials based on the new dithieno[3,2-*c*:2′,3′-*e*]-2,7-diketophosphepin (**DTDKP**) building block have been studied for the first time. Theoretical calculations predict **DTDKP** to be a better electron acceptor than the well-known dithienophosphole and the nitrogen analogue, bithiopheneimide. Cyclic voltammetry studies revealed two reduction processes that support their promising electron-acceptor properties, and modification of the P center with O or gold(I) further reduced the LUMO energy to ca. −3.6 eV. Expansion of the **DTDKP** core with various aromatic moieties has been realized using the Huisgen alkynyl click reaction, resulting in altered optical and electrochemical properties with compounds showing a high-energy absorption band at ca. 270−290 nm and a low-energy band at ca. 390−460 nm. The acceptor character of the **DTDKP** core was demonstrated by a red shift following the electron-donating strength of the appended aromatic moiety. Intriguing white-light emission from just a single species with the CIE coordinates of (0.33, 0.34) was observed for some of the extended species as the result of an unexpected dual-emission behavior. The high-energy emission in the blue-to-green region and the low-energy emission in the orange-to-red region are attributed to a $\pi^* \rightarrow \pi$ transition of the **DTDKP** core and charge transfer from the triazole moiety to **DTDKP**, respectively. Apart from tuning of the molecular properties, this novel building block has also been applied in a self-assembled organogel, which exhibited pronounced luminescence. Scanning electron microscopy confirmed that the gel self-assembled by forming a network of entangled 1D fibrous structures on the micrometer scale.

INTRODUCTION

Organic conjugated materials have recently drawn increasing attention because of their utility for important applications in sustainable and low-cost electronic devices such as organic photovoltaics (OPVs),[1] organic light-emitting diodes (OLEDs),[2] and organic field-effect transistors (OFETs).[3] To function efficiently, these devices require two complementary semiconductor components: a p-type component that can conduct positive charges or holes and an n-type component for negative charge transport. Extensive efforts in the past have been focused on the development of p-type semiconductor materials;[4] however, the number of n-type materials is quite limited.[5] Therefore, the development of new n-type materials is a highly rewarding direction for improving the performances of organic electronics. One of the key parameters for evaluating the n-type properties of materials is the lowest unoccupied molecular orbital (LUMO) energy. Materials with low LUMO energies have high electron affinities and could also enhance the electron transport. A widely used strategy to lower the LUMO energy is the introduction of an electron-withdrawing moiety such as a carbonyl,[6] cyano,[7] pentafluoro,[8] trifluoromethyl,[9] or imide[10] group into the organic framework.

On the other hand, the incorporation of inorganic main-group elements, particularly B,[11] Si,[12] and P,[13] in π-conjugated materials has recently created new avenues leading to materials for energy applications that also show some unique properties. Because of the versatile reactivity and electronic nature of phosphorus, organophosphorus materials offer considerable promise for the development of new functional materials with novel properties and provide a broad range of facile possibilities for efficient modification of the electronic properties of the product materials. As a prominent representative of this family, phosphole-based conjugated systems have attracted significant attention. Systematic groundbreaking studies by others and our group revealed that the LUMO energies of the phosphole derivatives can be stabilized through $\sigma^*-\pi^*$ orbital coupling, making phosphole-based materials very promising electron-acceptor materials.[13−18] One intriguing example is the dithienophosphole system (Chart 1), a very strong blue-light emitter with photoluminescence efficiencies of up to 90% that was developed by us in 2004.[14a] Most importantly, the photophysical properties can be easily tuned by the introduction of electron-donating or electron-accepting moieties on the scaffold or by simple modification of the phosphorus center (e.g., E = lone pair, O, S, Me^+, BH_3, or a

Received: November 1, 2012
Published: January 11, 2013

   dx.doi.org/10.1021/ja310680x | *J. Am. Chem. Soc.* 2013, 135, 1137−1147

Chart 1. (a) Molecular Design of the Target Dithieno[3,2-*c*:2′,3′-*e*]-2,7-diketophosphepin (DTDKP) by Hybridization of Dithienophosphole and Bithiopheneimide (BTI); (b) Examples of Cyclic Diketophosphanyl Compounds

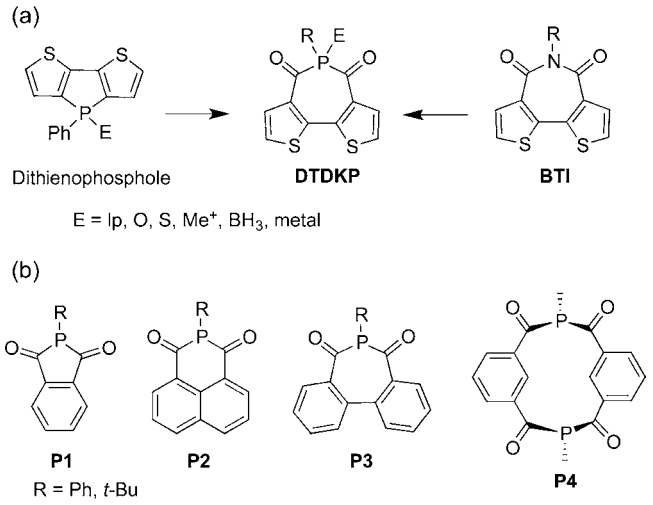

metal).[14] Very recently, our group reported a series of strongly electron-accepting organophospholes formed by introducing nitrogen atoms into the dibenzophosphole framework, some of which exhibited remarkably low reduction potentials of ca. −0.51 V, demonstrating the exceptional benefits derived from the electron-withdrawing nature of the phosphole materials.[14h,i]

In 2008, Facchetti, Marks, and co-workers reported an excellent n-type building block, bithiopheneimide (**BTI**, Chart 1), which has successfully been applied in conjugated homopolymers and donor−acceptor (D−A) copolymers for high-performance OFETs and OPVs.[19] Replacement of the nitrogen atom in **BTI** with phosphorus would provide the novel phosphorus-containing building block dithieno[3,2-*c*:2′,3′-*e*]-2,7-diketophosphepin (**DTDKP**) (Chart 1). In contrast to **BTI**, the energy levels of the novel **DTDKP** should be further tunable by simple modification of the phosphorus center (Chart 1), potentially enhancing the value of this building block over its N analogue. As a guide for experimental studies, preliminary theoretical calculations (vide infra) showed that these P species indeed exhibit lower LUMO energies and that subsequent oxidation of the P center further decreases the LUMO energy and consequently further increases its acceptor character. The novel compounds can also be deemed "next-generation" dithienophospholes as a result of the introduction of the two carbonyl groups, which have successfully been established to induce n-type features.

In this contribution, we now present the synthesis and characterization of **DTDKP** and demonstrate its successful application in the construction of conjugated materials. **DTDKP**'s photophysical properties can be further tuned by the use of combinations of various aromatics with different electronic properties and simple modification of the phosphorus center. In addition, the attachment of long alkoxy chains provides the potential for intermolecular hydrophobic−hydrophobic interactions as a driving force for aggregation at the microscale, with the goal of improving **DTDKP**'s materials properties via a self-assembly approach.

RESULTS AND DISCUSSION

Synthesis. Literature reports on cyclic diketophosphanyl systems are very limited, and the first few examples (**P1**−**P3** in Chart 1) were reported by Cowley and co-workers back in 1987.[20a] However, it was not until 2004 that the first X-ray structure of this class of cyclic compounds (**P1**) was reported.[20b] Very recently, Crossley and co-workers reported another interesting example that deals with the self-assembly of diphosphametacyclophane **P4**.[20c] To the best of our knowledge, these four species represent the comprehensive list of cyclic systems with a diketophosphanyl moiety.

The synthetic routes toward two basic diketophosphepins **1** and **2** are shown in Scheme 1. The key intermediate $PhP(SiMe_3)_2$ was synthesized according to a modification of a reported procedure via the reaction of $PhPH_2$ with Me_3SiOTf in the presence of Et_3N at room temperature overnight.[21] Because of its highly air- and moisture-sensitive nature, $PhP(SiMe_3)_2$ was prepared in situ for the next step. The synthesis of 3,3′-dicarboxylic acid-5,5′-bisalkynyl-2,2′-bithiophene (**S2**) was adapted from the known procedure leading to **S1** (Scheme 1).[19a] Alkynylation of 3,3′,5,5′-tetrabromo-2,2′-bithiophene with TMS−C≡CH in the presence of $PdCl_2(PPh_3)_2$, CuI, and PPh_3 in *i*-Pr_2NH gave 3,3′-dibromo-5,5′-bis(trimethylsilylacetylenyl)-2,2′-bithiophene (**S3**). To obtain the corresponding dicarboxylic acid, slow addition of *n*BuLi to the THF solution of **S3** followed by quenching of the dilithiated salt with dry CO_2 and subsequent desilylation using KOH in one pot afforded the dilithiated salt of 3,3′-dicarboxylate-5,5′-bisalkynyl-2,2′-bithiophene; **S2** was finally obtained by acidification using dilute HCl. The corresponding diacid chlorides of **S1** and **S2** were synthesized by reacting the diacid derivatives with oxalyl chloride at room temperature

Scheme 1. Synthesis of DTDKPs

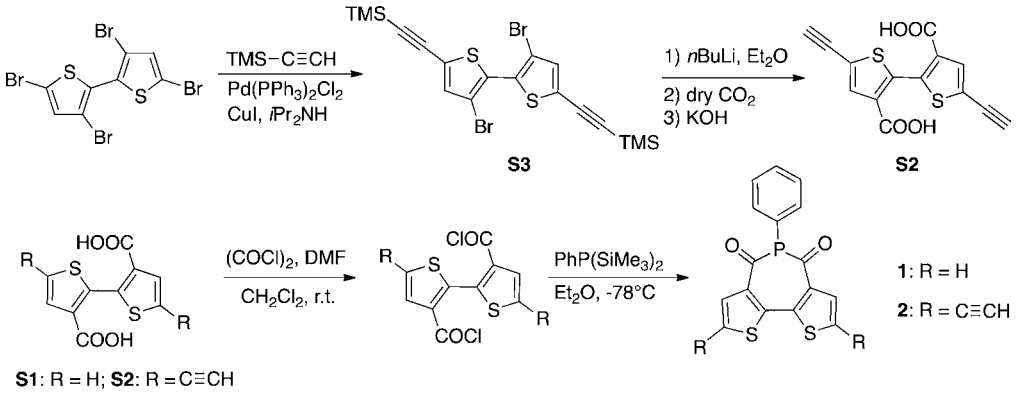

dx.doi.org/10.1021/ja310680x | J. Am. Chem. Soc. 2013, 135, 1137−1147

Scheme 2. Synthesis of Compounds 3–6 by the Huisgen Alkynyl–Azide Click Reaction

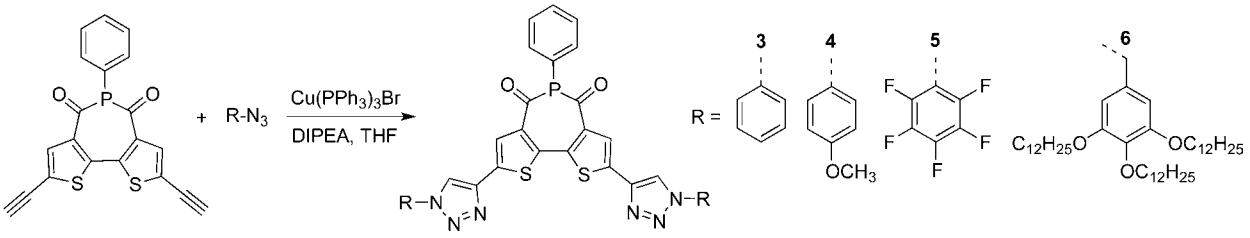

without further purification. Finally, formation of the cyclic **DTDKPs** was achieved by reaction of the diacid chlorides with $PhP(SiMe_3)_2$ in Et_2O at −78 °C according to a literature report on a somewhat related system (Scheme 1).[20a] Both **1** and **2** were fully characterized by ^1H, ^{13}C, and ^{31}P NMR spectroscopy, high-resolution mass spectrometry (HRMS), and elemental analysis. The structures of **1** and **2** were furthermore confirmed by single-crystal X-ray crystallography (vide infra).

For further extension of the conjugation of the basic framework, our initial efforts focused on the synthesis of a dibrominated **DTDKP** for subsequent cross-coupling reactions using *N*-bromosuccinimide under various conditions (e.g., in $CHCl_3$/AcOH, *N*,*N*-dimethylformamide, or trifluoroacetic acid/H_2SO_4); however, all attempts were met with failure. One possible reason for this behavior could be the strong electron-accepting character of **DTDKP**, which likely inhibits electrophilic bromination of the scaffold. Consequently, compound **2** with two terminal alkynyl groups was identified as a suitable target species for the Huisgen alkynyl–azide "click" reaction, which has also been widely used in the construction of organic conjugated materials because of its ease of synthesis, high functional group tolerance, and excellent reaction yields.[22]

Subsequently, click reactions were run using $Cu(PPh_3)_3Br$ as the catalyst in the presence of *N*,*N*-diisopropylethylamine (DIPEA) as the base in tetrahydrofuran (THF) solution at room temperature for 48 h (Scheme 2).[23] The organic-soluble and air-stable $Cu(PPh_3)_3Br$ catalyst not only allowed for homogeneous reaction conditions, thereby increasing the efficiency, but also avoided Cu coordination of the P center in the trivalent diketophosphepin, which potentially could poison the catalyst and hamper the reaction process.

Notably, all of the trivalent compounds **1**–**6** are air- and moisture-stable, supporting a reduced Lewis basicity of the P center as well as reduced electrophilic character of the carbonyl groups. The thermal stability of the compounds was evaluated by thermogravimetric analysis (TGA) using four representative examples. The decomposition temperatures (defined as the temperatures of 5% mass loss) for **1**, **2**, **4**, and **5** were determined to be 245, 430, 300, and 220 °C, respectively, indicating modest-to-high thermal stability.

The ^{31}P NMR resonance signals of the compounds are located in the range 64–67 ppm, which are shifted significantly downfield from those of trivalent dithienophospholes (−20 ± 3 ppm).[14] On the basis of the limited available information, the strongly low-field-shifted ^{31}P NMR resonances of this new class of cyclic phosphorus compounds can be attributed to the ring size. The ring size of related cyclic organophosphanes has been found to lead to quite large shift variances between −28 and 74 ppm.[20a] A similar ring effect on the ^{31}P NMR resonance has also been observed in chelated phosphane–metal complexes.[24]

To elaborate on the potential reactivity of the trivalent phosphorus center of the diketophosphepin system, two typical modifications were carried out using **1** as representative example (Scheme 3). The conversion to **1-AuCl** was readily

Scheme 3. Modification of the Phosphorus Center in 1

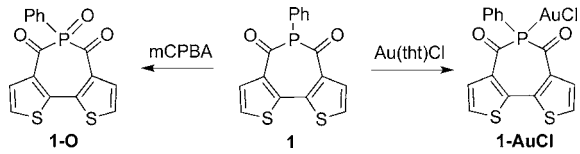

achieved by reaction with Au(tht)Cl (tht = tetrahydrothiophene) in CH_2Cl_2 at room temperature, according to our established procedures for the dithienophosphole system.[14] The successful conversion was confirmed by a distinct upfield shift in the ^{31}P NMR signal in going from **1** (64.6 ppm) to **1-AuCl** (49.5 ppm) as well as elemental analysis. This inverse chemical shift trend is contrary to what we expected[14] but can likely be attributed to conformation changes in the seven-membered ring induced by the modification of the P center.

In contrast to the dithienophosphole system, the synthesis of the oxide **1-O** occurred successfully only when *m*-chloroperoxybenzoic acid (mCPBA) was used as the oxidant. The application of conventional oxidation conditions, such as H_2O_2, *t*-BuOOH, or $NaIO_4$, led to quick decomposition into **S1**, as confirmed by NMR analysis. Remarkably, the reaction with mCPBA is very fast and evident by the immediate color change of the solution from yellow to red. A similarly abnormal upfield shift of the ^{31}P NMR signal for **1-O** at 10.5 ppm was also observed for this transformation.[14−18] Overall, while somewhat limited in this case, the reactivity of the P center nevertheless confirmed the important advantage of organophosphorus materials over other genuine organic systems and also their nitrogen counterparts.

X-ray Crystallography. Single crystals of **1** and **2** suitable for X-ray crystallography were obtained from slow evaporation of concentrated acetone solutions at room temperature. The molecular structures of **1** and **2** in the solid state are depicted in Figures 1 and 2, respectively. It should be noted that the structure of **2** showed some disorder arising from two out-of-plane positions of the P atom that consequently affected the position of the O atoms and the phenyl ring as well; Figure 2 shows only one of the conformations. The crystal data and structure refinement details are included in the Supporting Information (SI). In both cases, the two thiophene rings of the main scaffold are arranged in almost coplanar fashion, with small C3–C4–C5–C6 torsion angles of 1.4 and 7.5° for **1** and **2**, respectively. This highly planar conjugated character was also observed in the only X-ray-crystallographically characterized N analogue, which has a torsion angle of 4.3°.[19a] However, a distinct difference of **DTDKP** is that the P center is pyramidal, as would be expected.[14a−c] Moreover, the P atom is significantly twisted out of the plane, with interplanar angles (between the

dx.doi.org/10.1021/ja310680x | J. Am. Chem. Soc. 2013, 135, 1137–1147

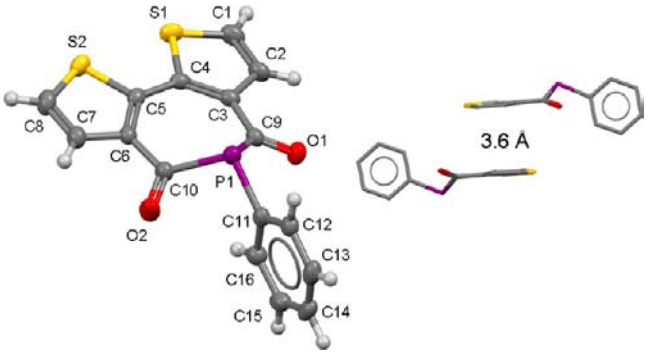

Figure 1. (left) Molecular structure of **1** (50% probability level) and (right) intermolecular interactions in the solid state. Selected bond lengths (Å) and angles (deg): P1−C9, 1.843(3); P1−C10, 1.848(2); P1−C11, 1.811(2); C3−C9, 1.469(3); C6−C10, 1.471(3); C9−O1, 1.219(3); C10−O2, 1.216(2); C1−C2, 1.351(4); C2−C3, 1.427(4); C3−C4, 1.381(4); C4−C5, 1.455(3); C5−C6, 1.381(3); C6−C7, 1.423(4); C7−C8, 1.342(4); C9−P1−O10, 107.9(1); C9−P1−C11, 100.7(1); C10−P1−C11, 102.1(1); C4−C3−C9, 129.0(2); C5−C6−C10, 128.9(3); C3−C9−P1, 121.8(2); C6−C10−P1, 120.6(2).

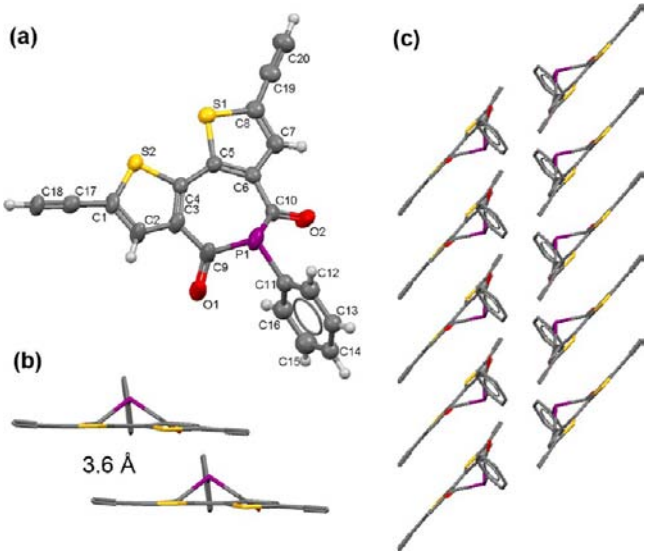

Figure 2. (a) Molecular structure of **2** in the solid state (50% probability level) and (b, c) its intermolecular packing. Only one of the disordered conformations is shown. Selected bond lengths (Å) and angles (deg): P1−C9, 1.756 (7); P1−C10, 1.946 (7); P1−C11, 1.798 (7); C3−C9, 1.502 (8); C6−C10, 1.478 (8); C9−O1, 1.309(1); C10−O2, 1.189(7); C1−C2, 1.352(8); C2−C3, 1.408(8); C3−C4, 1.363(8); C4−C5, 1.446(8); C5−C6, 1.388(8); C6−C7, 1.406(8); C7−C8, 1.358(9); C8−C19, 1.413(9); C19−C20, 1.175(9); C1−C17, 1.432(8); C17−C18, 1.178(8); C9−P1−O10, 101.3(3); C9−P1−C11, 105.9(5); C10−P1−C11, 101.2(5); C4−C3−C9, 128.7(5); C5−C6−C10, 129.1(5); C3−C9−P1, 120.0(5).

C9−P1−C10 and C3−C4−C5−C6 planes) of 47.9 and 59.6° for **1** and **2**, respectively; this is in contrast to the in-plane P atom of the dithienophosphole system.[14a−c] The rotation about the exocyclic P−C bond results in an almost orthogonal orientation of the phenyl ring with respect to the bithiophene moiety. The two endocyclic P−C bonds were determined to be 1.843(3) and 1.848(2) Å in **1** and 1.756(7) and 1.946(8) Å in **2**, while the exocyclic P−C bond lengths for **1** and **2** are 1.811(2) and 1.798(7) Å, respectively. This trend is inverse to the one in the dithienophosphole system, where the endocyclic bonds are slightly shorter than the exocyclic one, and can be attributed to the geometric strains resulting from the different ring sizes rather than to a lack of the conjugation.[14a] The lengths of endocyclic P−C bonds in **1** and **2** are comparable to those reported for **P1** (ca. 1.85 Å)[20b] and **P4** (ca. 1.89 Å)[20c] and clearly longer than the average P=C bond in phosphaalkenes (1.61−1.71 Å), suggesting the absence of full delocalization of the phosphorus lone pair toward the carbonyl groups.[25] For compound **2**, two terminal alkynyl groups are clearly present, showing C≡C bond lengths of 1.175(9) and 1.178(8) Å, and the bond angles of the sp-hybridized carbon are close to the ideal value of 180°.

Both compounds **1** and **2** show weak intermolecular $\pi-\pi$ stacking interactions at a distance of ca. 3.6 Å (Figures 1 and 2), but their respective molecular packing modes are different. Compound **1** exhibits obvious inverse face-to-face interactions between the bithiophene planes with almost complete overlap of the scaffolds of neighboring molecules. For **2**, neighboring molecules show the same orientation of the P centers, with only partial overlap of bithiophene planes as a consequence of the steric bulk of the phosphanyl groups. However, this slipped-stacking mode does not preclude the formation of a well-ordered one-dimensional (1D) organization (Figure 2c).

Photophysical Properties. The UV−vis spectra of compounds **1**−**5** in CH_2Cl_2 are depicted in Figure 3, and the

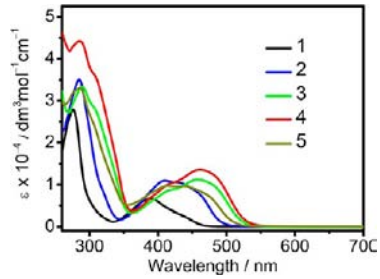

Figure 3. UV−vis spectra of **1**−**5** in CH_2Cl_2.

photophysical data are shown in Table 1. All of the compounds show a high-energy absorption band at ca. 270−290 nm and a low-energy band at ca. 390−460 nm. Compared with **1**, the extended conjugated species **2**−**5** show lower-energy absorption bands and higher extinction coefficients. The absorption data indicate narrower HOMO−LUMO energy gaps for the extended species, which is in line with the results of theoretical calculations (vide infra).

Attachment of the various aromatic moieties with different electronic properties in **3**−**5** was found to show the expected effect on the absorption maximum (λ_{max}) and onset of the UV−vis absorption spectra. The trend in λ_{max}, **4** (461 nm) > **3** (458 nm) > **5** (440 nm), is consistent with the electron-donating abilities of the aromatic moieties, **4** (p-C_6H_4-OMe) > **3** (Ph) > **5** (C_6F_5), clearly supporting the electron-accepting ability of the diketophosphepin moiety and consequently a donor−acceptor−donor architecture.[26]

While species **1** and **2** show blue-to-green emissions with maxima at λ_{em} = 468 and 492 nm that can be attributed to the $\pi^* \rightarrow \pi$ transition of the **DTDKP** core (see the SI), some intriguing unexpected excitation-dependent luminescence behavior was observed for **3**−**5**. In addition, molecules **3**−**5** with more extended π systems have larger quantum yields than **1** and **2**. Figure 4a shows the UV−vis absorption spectrum and

dx.doi.org/10.1021/ja310680x | J. Am. Chem. Soc. 2013, 135, 1137−1147

Table 1. Photophysical, Electrochemical, and Calculated Data for 1−6

				electrochemistry		calculated/eV		
compd	λ_{abs}/nm[a] (ε/dm^3 mol^{-1} cm^{-1})	λ_{em}/nm (Φ_F) (CH_2Cl_2)	λ_{em}/nm (solid)	$E_{red,1/2}$/V[d]	E_{LUMO}/eV[e]	E_{LUMO}	E_{HOMO}	E_g[f]
1	276 (27870), 390 (6650)	468 (0.02)[b]	NA	E_{red1} = −1.66 E_{red2} = −1.95	−3.14	−2.66	−6.06	3.40
1-O	283 (17152), 422 (4859)	470	NA	E_{red1} = −1.17 E_{red2} = −1.65	−3.63	−3.21	−6.18	2.97
1-AuCl	294 (15800), 411 (4475), 460sh (3000)	586 (0.10)[c]	578	E_{red1} = −1.15 E_{red2} = −1.59 E_{red3} = −1.99	−3.65	−3.74	−6.74	3.00
2	285 (35053), 410 (10945)	492 (0.03)[b]	NA	E_{red1} = −1.42 E_{red2} = −1.73	−3.38	−2.93	−5.98	3.05
3	289 (33315), 458 (11172)	592 (0.08)[c]	NA	NA	NA	−2.79	−5.66	2.87
4	285 (44178), 461 (13528)	599 (0.10)[c]	617	NA	NA	−2.78	−5.60	2.82
5	286 (33033), 411 (9717), 440 (9623)	485 (0.15)[c]	630	E_{red1} = −1.45 E_{red2} = −1.72	−3.35	−2.85	−5.77	2.92
6	285 (35012), 461 (11454)	598 (0.09)[c]	582, 635 (sh)	E_{red1} = −1.53 E_{red2} = −1.86	−3.27	NA	NA	NA
BTI	NA	NA	NA	NA	NA	−2.32	−6.18	3.86

[a]In CH_2Cl_2. [b]Photoluminescence quantum yield in CH_2Cl_2 relative to quinine sulfate. [c]Photoluminescence quantum yield in CH_2Cl_2 relative to fluorescein. [d]Potentials vs ferrocene/ferrocenium (Fc/Fc^+). [e]Calculated using the Fc HOMO level at $-(4.8 + E_{red,1/2})$ eV. [f]$E_g = E_{LUMO} - E_{HOMO}$.

excitation and emission spectra (excited at different wavelengths) of **4** in CH_2Cl_2.

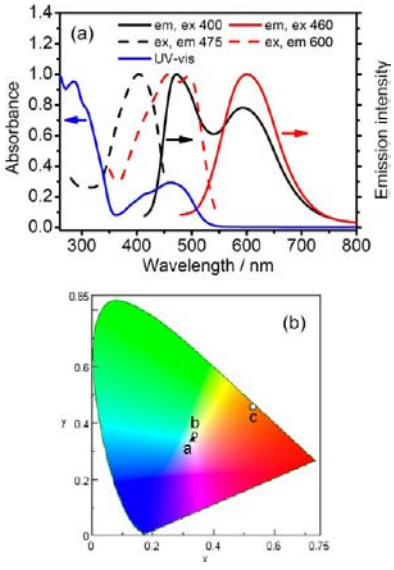

Figure 4. (a) UV−vis absorption spectrum (solid blue), emission spectra (solid black and red), and excitation spectra (dashed black and red) of **4** in CH_2Cl_2. (b) CIE coordinates for photoluminescence of **4** excited at different wavelengths [a: λ_{ex} = 365 nm, CIE (0.33, 0.34); b: λ_{ex} = 400 nm, CIE (0.33, 0.36); c: λ_{ex} = 460 nm, CIE (0.53, 0.46)].

Upon excitation at λ_{ex} = 365 nm, white photoluminescence with dual emission bands at λ_{em} = 475 and 600 nm with an intensity ratio (I_{475}/I_{600}) of 1.30 was observed. The complementary colors of blue-green (475 nm) and orange (600 nm) in one single molecule contribute to the intriguing white-light emission. To characterize the white-light emission, the commonly used Commission International de l'Eclairage (CIE) coordinates were determined to be (0.33, 0.34), which is very close to those of pure white light, (0.33, 0.33) (Figure 4b).[14d] Remarkably, excitation at longer wavelength (λ_{ex} = 460 nm) led to exclusively orange emission with CIE coordinates of (0.53, 0.46). These results are intriguing insofar as white-light emission is generally obtained using strategies based on additive color mixing by combining different luminophores through covalent linkages or via self-assembly approaches;[27a] single molecules that exhibit white-light emission remain rare to date.[27b,c]

Detailed excitation studies revealed that the high- and the low-energy emissions originate from different states (Figure 4). The higher-energy emission, derived from a featureless excitation at ca. 399−404 nm, is attributed to the $\pi^* \rightarrow \pi$ transition of the core similar to those of **1** and **2**. The low-energy emission band, derived from an excitation band at ca. 453−495 with a shape similar to the low-energy absorption band, is tentatively assigned to charge transfer from the peripheral aromatic part to the **DTDKP** core.[28] The dual emissions are attributed mainly due to a twisted structure in solution.[28] Similar dual-emission behavior was also observed for **3**, for which the ratio of the intensities of the high- and low-energy emissions (I_H/I_L) is 1.28 (λ_{ex} = 400 nm; see the SI). For compound **5**, however, the high-energy emission is predominant (I_H/I_L = 4.46, λ_{ex} = 400 nm). It is plausible that the electron-accepting C_6F_5 group stabilizes the energy levels, making the charge-transfer emission in the low-energy region less favorable (see the SI).[28]

In the solid state, photoexcitation at either high (λ_{ex} = 365 nm) or low energy (λ_{ex} = 450−520 nm) produced only a single low-energy emission at λ_{em} = 617 and 630 nm for **4** and **5**, respectively, suggesting the suppression of the twisted structure, which allows the charge-transfer process to be more dominant (see the SI). The red-shifted emissions in the solid state also suggest more efficient conjugation due to the planarity of the molecules. In contrast to **4**, however, **5** with the electron-accepting C_6F_5 moiety exhibits a more pronounced low-energy emission, which can be attributed to the presence of intramolecular F···H hydrogen-bonding interactions (see the SI). Although weak in solution, such intramolecular six-membered-ring F···H hydrogen-bonding interactions have very recently been reported to be an important non-covalent solid-state force for triazole systems.[29]

dx.doi.org/10.1021/ja310680x | J. Am. Chem. Soc. 2013, 135, 1137−1147

To support the presence of a charge-transfer transition in compound **4**, solvatochromic absorption and emission studies in representative solvents of different polarity (hexanes, CH_2Cl_2, and CH_3OH) were carried out. As shown in Figure 5, the low-energy emission was clearly red-shifted from 600 to

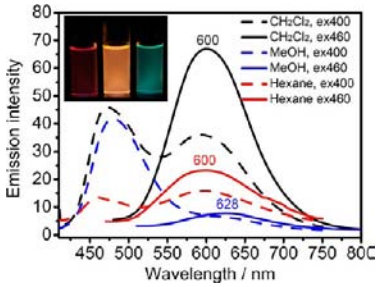

Figure 5. Effect of the solvent on the emission spectra of **4**. Inset: photograph of emission in different solvents (from left to right: hexane, CH_2Cl_2, and MeOH).

628 nm, as the solvent was changed from dichloromethane to methanol. Most interestingly, three distinct emission colors (red, yellow, and green) were observed in different solvents with increasing polarity (hexanes, CH_2Cl_2, and MeOH, respectively) as a result of the I_H/I_L ratios (hexane: I_H/I_L = 0.86; CH_2Cl_2: I_H/I_L = 1.29; MeOH: I_H/I_L = 6.60). The polar methanol likely forms hydrogen bonds with a N atom of the triazole moiety, thereby interrupting the coplanarity of the conjugated backbone, which minimizes the low-energy emission band in favor of the dominant high-energy band. On the other hand, the solubility of **4** is diminished in hexanes, and the corresponding photophysics likely the result of aggregation. Consequently, the observed low-energy red emission results from extended π conjugation due to the planarized scaffold in the aggregates. Notably, aggregation is further supported by the observation that when the hexane solution of **4** was allowed to sit for ca. 1 h, a precipitate formed that showed the same red emission in the solid state as was observed for its solution.

As mentioned previously, one unique advantage of organophosphorus materials is that their photophysics is tunable by simple modification of the P center. Indeed, modification of phosphorus with O or Au(I) produced considerable UV–vis absorption and emission changes. Generally, oxidation of the trivalent compounds results in a red-shifted absorption due to the lowered HOMO–LUMO gap. A representative example of UV–vis changes upon oxidation is shown in Figure 6. Upon addition of mCPBA, the spectrum of **1** overall underwent a red shift, accompanied by decreases in the bands at ca. 276 and 390

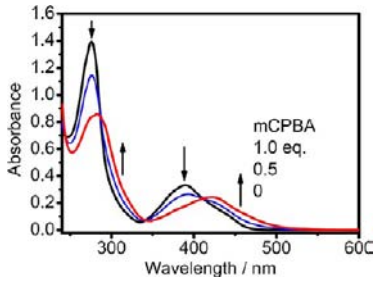

Figure 6. UV–vis spectral changes of **1** upon addition of mCPBA in CH_2Cl_2.

nm and the concomitant formation of new bands at 283 and 422 nm. Three isosbestic points at ca. 287, 341, and 411 nm were observed, suggesting the clean transformation of **1** into **1-O**. The conversion was very fast and complete upon addition of 1 equiv of mCPBA (see the SI), which is in line with the NMR spectroscopic studies (vide supra). Similar red shifts were also observed in the UV–vis absorption spectra of **2**–**5** upon oxidation (see the SI). Moreover, red shifts in the emission bands by about $\Delta\lambda_{em}$ = 70 nm were also observed for the more conjugated molecules **3**–**5** (see the SI), indicating the high synthetic value of P modification for narrowing the HOMO–LUMO energy gap of conjugated materials.

Apart from phosphorus oxidation, the formation of the gold(I) complex of **1** resulted in a similar red shift of the UV–vis absorption (see the SI). Strikingly, the gold(I) complex **1-AuCl** also showed dual-emission behavior. Excitation at λ_{ex} = 365 or 380 nm produced a high-energy emission at λ_{em} = 450 nm and a low-energy emission at λ_{em} = 585 nm with I_H/I_L = 0.73 or 0.29, respectively (Figure 7). However, excitation at

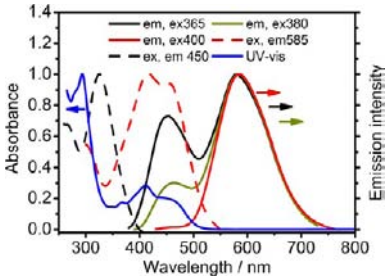

Figure 7. Emission spectra of **1-AuCl** excited at different wavelengths in CH_2Cl_2.

longer wavelength (λ_{ex} = 400 nm) produced only one emission at λ_{em} = 585 nm. On the other hand, no significant solvent-dependent emission was observed for **1-AuCl**, and unlike **4** and **5**, the solid-state emission of **1-AuCl** did not show any obvious red shift either. This indicates that next to the absence of π–π interactions, aurophilic interactions that usually lead to lower-energy luminescence do not exist because of the bulky phosphorus center.[30] On the basis of the above facts and the results of theoretical calculations (vide infra), the two emissions are assigned to the metal-perturbed $\pi^* \rightarrow \pi$ transition of the **DTDKP** core and charge transfer from the lone pair of the Cl to **DTDKP**, respectively.

Electrochemistry. The electrochemical features of the new **DTDKP**s were determined by cyclic voltammetry to solidify further the electron-accepting character of the new system. To our satisfaction, each trivalent compound showed two quasi-reversible reduction peaks, and no oxidation peak was observed. The electrochemical data are summarized in Table 1, and representative cyclic voltammograms of compounds, **1**, **2**, and **5** are shown in Figure 8a. The first reduction peaks of **1**, **2**, and **5** were determined to be E_{red1} = −1.66, −1.42, and −1.45 V, respectively. With ferrocene as an internal reference, the LUMO energies (E_{LUMO}) of **1**, **2**, and **5** were determined from the first reduction peaks to be −3.14, −3.38, and −3.35 eV [$E_{LUMO} = -(E_{red1} + 4.8)$ eV].[31] Because of the relatively low solubility of **3** and **4** in CH_2Cl_2, the cyclic voltammograms of these two compounds were not accessible.

Interestingly, simple modification of **1** and **2** with gold(I) or O significantly decreased the reduction potentials, and two irreversible (or quasi-reversible) reduction peaks can be seen

dx.doi.org/10.1021/ja310680x | J. Am. Chem. Soc. 2013, 135, 1137–1147

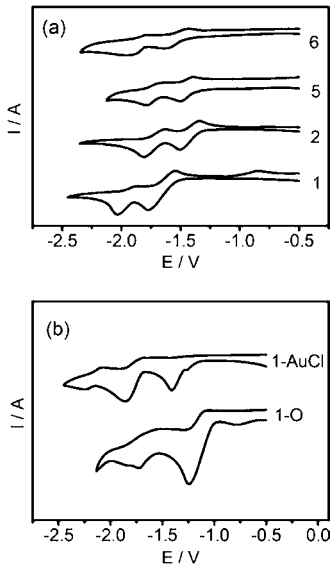

Figure 8. Cyclic voltammograms of (a) the trivalent compounds **1**, **2**, **5**, and **6** and (b) **1-O** and **1-AuCl** obtained from **1** by modification of the P center, recorded in CH_2Cl_2 solution containing 0.1 M tetrabutylammonium hexafluorophosphate as the supporting electrolyte. Scan rate = 100 mV/s. Ferrocene was added as an internal standard and referenced to 0 V.

(Figure 8b). The LUMO energies of **1-AuCl**, **1-O**, and **2-O** are E_{LUMO} = −3.65, −3.63, and −3.85 eV, respectively, suggesting that they have a considerably stronger electron-accepting character than their trivalent counterparts. These low-lying LUMOs are comparable to that of PCBM-C_{60} (E_{LUMO} = −3.7 eV),[32] which is a common electron acceptor in organic electronics.

DFT Calculations. To obtain a better understanding of the photophysical and electronic properties, density functional theory (DFT) calculations were performed using the Gaussian 09 suite of programs at the B3LYP level of theory with the 6-31G+(d) basis set for **1**−**5** and **1-O** and the LANL2DZ basis set for **1-AuCl**.[33] The coordinates for the optimized geometries of these compounds are included in the SI. The HOMO and LUMO orbital diagrams and energy levels are shown in Figures 9 and 10 and Table 1.

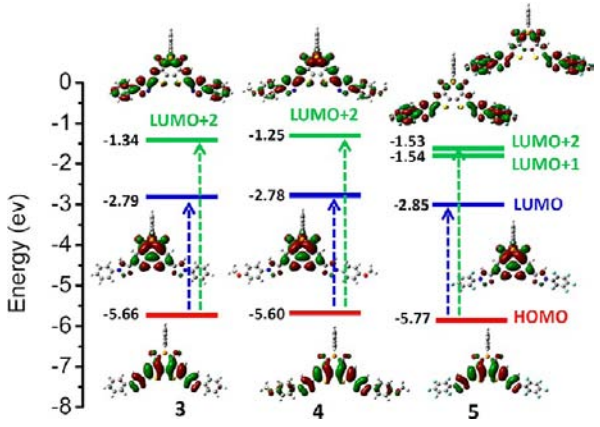

Figure 10. Frontier molecular orbital diagrams and the electronic transitions calculated using TD-DFT for **3**−**5**.

The HOMO of **1** mainly represents the π system of the bithiophene section of the **DTDKP** core. With further extension of the core, the electron density of the HOMO is considerably delocalized over the extended conjugated system in compounds **2**−**5**. The electron-donating methoxyphenyl group in **4** shows a larger contribution to the HOMO than the electron-accepting C_6F_5 group in **5**, supporting the expectedly stronger donor−acceptor interaction in **3**. The LUMOs of **1**−**5** mainly reside on the π^* orbital of the **DTDKP** core, with hyperconjugation between the σ^* orbital of the exocyclic P−C bond. Such a $\sigma^*-\pi^*$ interaction is typical for organo-

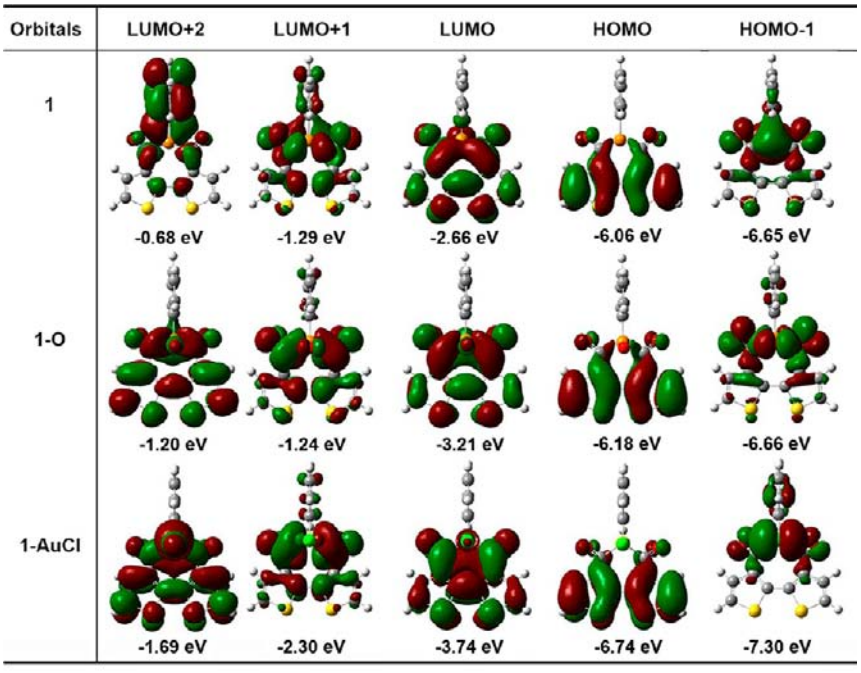

Figure 9. Frontier molecular orbitals for **1**, **1-O**, and **1-AuCl**.

dx.doi.org/10.1021/ja310680x | J. Am. Chem. Soc. 2013, 135, 1137−1147

Table 2. TD-DFT-Calculated Transition Data for 1−5[a]

	1	1-O	1-AuCl	2	3	4	5
λ/nm (f)[b]	440 (0.11)	496 (0.10)	507 (0.11)	484 (0.31)	519 (0.51)	527 (0.52)	507 (0.48)
transitions[c]	H → L (75%)	H → L (51%)	H → L (89%)	H → L (80%)	H → L (84%)	H → L (85%)	H → L (84%)
		H−1 → L (35%)					
λ/nm (f)[b]	286 (0.25)	321 (0.12)	314 (0.21)	302 (0.30)	323 (0.57)	325 (0.67)	329 (0.41)
transitions[c]	H → L+2 (17%)	H → L+1 (8%)	H → L+1 (32%)	H → L+2 (73%)	H → L+2 (69%)	H → L+2 (67%)	H → L+1 (77%)
	H−6 → L (65%)	H−6 → L (71%)	H−9 → L (29%)				
			H−8 → L (29%)				

[a]H = HOMO; L = LUMO. [b]f = oscillator strength. [c]The coefficient percentages of the orbitals involved in the transitions are given in parentheses.

phosphorus molecules and contributes to lowering the LUMO energy.[13]

The HOMOs and LUMOs of **1-O** and **1-AuCl** are quite similar to those of **1** and represent the π and π^* systems, respectively. It should be noted in this context that one lone pair of the chloride in **1-AuCl** contributes considerably to the HOMO−1 level, which is an important feature for the observed photophysics of **1-AuCl**. The HOMO and LUMO energies of **1** are E_{HOMO} = −6.06 eV and E_{LUMO} = −2.66 eV, respectively. It is noteworthy that **1** has a much lower LUMO energy than its nitrogen analogue **BTI** (E_{HOMO} = −6.18 eV, E_{LUMO} = −2.32 eV),[34] which can be attributed to the σ^*−π^* interaction discussed above, highlighting the promising advantage of organophosphorus materials. Incorporation of the π-conjugated moieties in the scaffolds of **2**−**5** stabilizes the LUMO (ΔE_{LUMO} for **2**−**5** = −0.27, −0.13, −0.12, and −0.19 eV, respectively) and destabilizes the HOMO (ΔE_{HOMO} for **2**−**5** = 0.08, 0.40, 0.46, and 0.29 eV, respectively), resulting in an overall decrease in the energy gap (E_g), as is commonly observed for conjugated materials. E_g follows the trend **4** (2.82 eV) < **3** (2.87 eV) < **5** (2.92 eV) < **2** (3.05 eV) < **1** (3.40 eV), which is consistent with the trend observed by UV−vis spectroscopy. Among the trivalent compounds, **2** exhibits the lowest LUMO energy because of the electron-accepting features of the alkynyl groups. In line with the electrochemistry results, modification of the phosphorus center significantly lowers the LUMO energy of **1** (ΔE_{LUMO} = −0.55 eV for **1-O** and ΔE_{LUMO} = −1.08 eV for **1-AuCl**), further confirming the strong electron-accepting nature of the modified **DTDKP**.

To gain a better understanding of the optical absorption properties, time-dependent DFT (TD-DFT) calculations were carried out subsequently.[35] The contributions of the molecular orbitals involved in the UV−vis transitions were determined on the basis of their oscillator strengths (f). The first 20 singlet and triplet states were calculated. The calculated transitions were consistent with the experimental data. The assignments of the transitions and the corresponding molecular orbital diagrams are shown in Table 2 and Figure 10.

Importantly, the composition of the frontier orbitals and the narrower energy gaps provide theoretical proof for the intriguing dual emissions of compounds **3**−**5** and **1-AuCl**. The reduced HOMO−LUMO energy gap due to the extension of the **DTDKP** core and modification of the P center results in lower-energy emissions at λ_{em} = 577−599 nm that can be attributed to charge transfer from the peripheral moieties (particularly the triazole unit) to the **DTDKP** core in **3**−**5** and the $\pi \rightarrow \pi^*$ transition of the **DTDKP** core in **1-AuCl**. As a result of the ring twist in solution, high-energy photoexcitation of **3**−**5** also produces short-wavelength emissions at λ_{em} = 473−485 exclusively from the **DTDKP** core, which are very likely suppressed in the solid state. For **1-AuCl**, the high-energy emission is due to ligand-to-ligand charge transfer from the lone pair of the Cl ligand that is involved in the HOMO−1 orbital to the π^* orbital of the **DTDKP.**

The TD-DFT calculations for the trivalent compounds **1**−**5** indeed predict low- and high-energy absorption bands for each compound (see Table 2). The low-energy absorptions mainly involve the HOMO → LUMO ($\pi \rightarrow \pi^*$) transition. The high-energy absorptions involve the HOMO → LUMO+2 transition for **1**−**4** and the HOMO → LUMO+1 transition for **5**, composed of the π^* orbital of the phenyl and triazole moieties. Overall, the theoretical calculations fully support the electrochemical and photophysical properties of these novel molecules.

Gelation Study. Next to the successful design of small molecules based on **2**, further attachment of self-assembly groups was applied in hopes of accessing features of self-assembly materials.[36] To our satisfaction, compound **6** indeed formed an organogel in hydrocarbon solvents (hexane or heptanes), as shown in Figure 11.

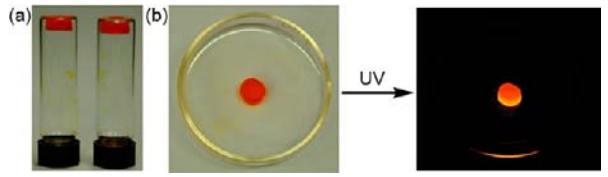

Figure 11. Photographs of (a) the organogels of **6** in (left) hexane and (right) heptane and (b) the orange photoluminescence of the organogel.

Gel formation required the heating of the heterogeneous mixture of **6** in the solvent to access a homogeneous solution phase that upon cooling formed an organogel. The critical gel concentration (CGC) was determined to be ca. 10 mg/mL in hexane and 8.5 mg/mL in heptane. Interestingly, upon cooling to room temperature, and in contrast to other traditional gels,[34] where the gelation process traps all of the solvent to form an inversion-stable soft material, a "gel island" of **6** in the solvent was observed that resulted from simple shrinking of the gel without any other morphological changes, akin to a sponge (Figure 11). The following gelation process of **6** involving two steps as shown in Scheme 4 is thus proposed: First, the solution of **6** forms a transparent metastable gel phase by trapping the hydrocarbon solvent in the interstitial network made up of **6**. Subsequently, this transparent gel network contracts upon cooling and expels some of the solvent molecules, likely as a result of stronger or more compatible hydrophobic interactions between the long alkoxy chains as well as π−π interactions between the rigid cores of the molecules of **6**, forming the final shrunken, stable gel phase.

dx.doi.org/10.1021/ja310680x | J. Am. Chem. Soc. 2013, 135, 1137−1147

Scheme 4. Proposed Process for the Self-Assembly of the Organogel of 6

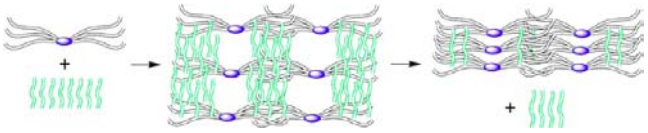

To confirm the self-assembly process and morphology further, scanning electron microscopy (SEM) was performed on xerogels (i.e., networks formed by the removal of solvent) of **6** obtained from hexane and heptanes and a solid sample obtained from evaporation of the dichloromethane solution. Interestingly, as shown in Figure 12, a network of microscopically entangled 1D fibers was observed for the xerogels (Figure 12 a–c), while no such fibril morphology was observed for the solid sample (Figure 12d), clearly supporting the self-assembly behavior of **6** in the gel phase. On the basis of the structure of **2** in the solid state determined by X-ray crystallography, it is inherently plausible that the conjugated backbone in **6** could form well-organized 1D $\pi-\pi$ stacks with the help of intermolecular hydrophobic interactions between the long alkoxy chains, resulting in the observed fibrous structures.

The photoluminescence properties of **6** in different states (solutions in hexane and CH_2Cl_2, gel from hexane, and solid) were also investigated (see the SI). In line with the other extended congeners **3**–**5**, a similar excitation-dependent emission was also observed for **6** in CH_2Cl_2. When excited at $\lambda_{ex} > 450$ nm, the emissions of **6** from hexane and CH_2Cl_2 solution and the gel state were determined to be $\lambda_{em} = 574$, 598, and 579 nm, respectively. The obvious red shift in CH_2Cl_2 relative to the other states suggests the charge-transfer character of the emission. Emission from the solid exhibited a lower-energy shoulder at 635 nm, suggesting the presence of intermolecular $\pi-\pi$ interactions. Compound **6** also showed two reduction processes ($E_{red1} = -1.53$, $E_{red2} = -1.86$ eV), in line with its relatives **3**–**5** (Figure 8), but they occurred at higher potentials than those of **5**, likely because of the interruption of the electronic connection between the triazole and phenyl groups.

CONCLUSIONS

A series of multifunctional conjugated materials **1**–**6** based on the novel **DTDKP** building block have been designed and synthesized, and their intriguing photophysical, electrochemical, and self-assembly properties have been established. The design of this new building block was inspired by our extensive research on the dithienophosphole system as well as the recently introduced electron acceptor **BTI**.

The new building block, **DTDKP**, exhibits promising electron-accepting character, as confirmed by theoretical calculations and electrochemistry, where two reduction processes were observed. By attaching various terminal aromatic groups with different electronic properties to the **DTDKP** core, conjugated compounds **2**–**6** were purposely designed. The extended structures feature red-shifted UV–vis absorption and emission spectra and consequently narrower HOMO–LUMO energy gaps. Because of twisting of the appended triazole units and the core in molecules **3**–**5**, photoexcitation at high energy leads to an intriguing dual-emission behavior, where the high-energy and low-energy emissions are attributed to the $\pi^* \rightarrow \pi$ transition of the **DTDKP** core and charge transfer from the triazole moiety to **DTDKP**, thereby producing white-light emission. As a synthetic advantage of organophosphorus materials, the phosphorus center of these molecules can easily be modified by oxidation and gold(I) complexation, leading significantly altered photophysics and electronics. In addition to tuning the intrinsic molecular properties of the building block, we could also successfully address extrinsic materials properties by incorporating self-assembly groups into the **DTDKP** core, leading to an interesting luminescent organogel of **6** with a microscopic 1D fiber structure.

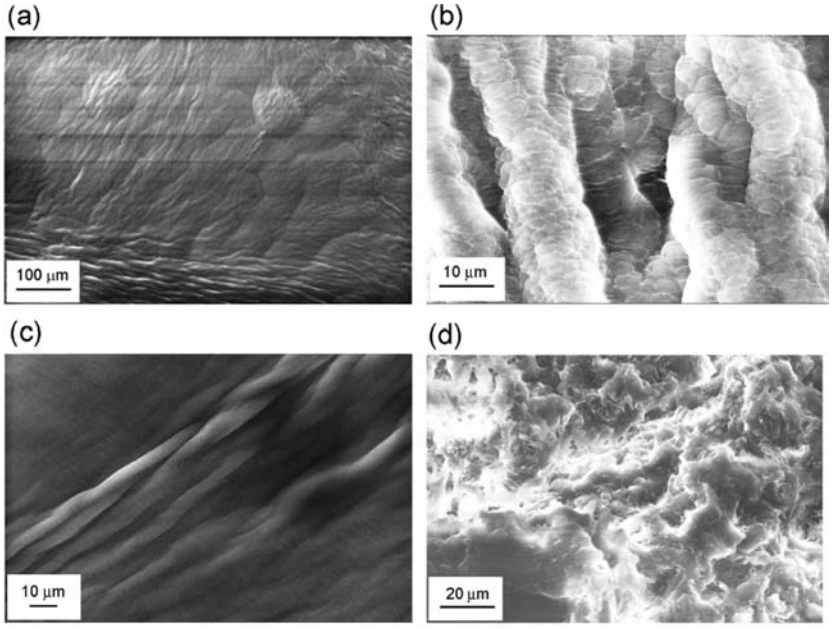

Figure 12. Variable-pressure SEM images of (a, b) a xerogel of **6** obtained from heptane, (c) a xerogel of **6** obtained from hexanes, and (d) solid **6** obtained from evaporation of CH_2Cl_2 (landing energy = 20 kV, ambient pressure = 30 Pa for all images).

dx.doi.org/10.1021/ja310680x | *J. Am. Chem. Soc.* 2013, 135, 1137–1147

In summary, a novel organophosphorus building block, **DTDKP**, has been designed and demonstrated to be valuable for applications involving multifunctional conjugated materials. Further detailed studies on the intriguing properties and potential applications of this new system are currently underway in our laboratory.

■ ASSOCIATED CONTENT

Supporting Information

Detailed experimental procedures; CIF files; crystal data and structure refinement for **1** and **2**; additional photophysical data; full characterization (^{1}H, ^{31}P, ^{13}C, and ^{19}F NMR) of **1**−**6**; optimized structure coordinates of **1**−**5**, **1-O**, and **1-AuCl**; and complete ref 33. This material is available free of charge via the Internet at http://pubs.acs.org.

■ AUTHOR INFORMATION

Corresponding Author

thomas.baumgartner@ucalgary.ca

Notes

The authors declare no competing financial interest.

■ ACKNOWLEDGMENTS

Financial support by NSERC of Canada, the Canada School for Energy and Environment, and the Canada Foundation for Innovation (CFI) is gratefully acknowledged. We thank Prof. Todd Sutherland for his kind help with the electrochemistry, J. B. Lin for helpful discussions regarding the X-ray crystal structure of **2**, and M. Stolar for her help with the TGA measurements.

■ REFERENCES

(1) (a) Günes, S.; Neugebauer, H.; Sariciftci, N. S. *Chem. Rev.* **2007**, *107*, 1324−1338. (b) Son, H. J.; He, F.; Carsten, B.; Yu, L. *J. Mater. Chem.* **2011**, *21*, 18934−18945. (c) Chen, J.; Cao, Y. *Acc. Chem. Res.* **2009**, *42*, 1709−1718.

(2) (a) Burn, P. L.; Lo, S. C.; Samuel, I. D. W. *Adv. Mater.* **2007**, *19*, 1675−1688. (b) *Organic Light Emitting Devices*; Müllen, K., Scherf, U., Eds.; Wiley-VCH: Weinheim, Germany, 2006.

(3) Ebata, H.; Izawa, T.; Miyazaki, E.; Takimiya, K.; Ikeda, M.; Kuwabara, H.; Yui, T. *J. Am. Chem. Soc.* **2007**, *129*, 15732−15733. (b) Anthony, J. E. *Angew. Chem., Int. Ed.* **2008**, *47*, 452−483.

(4) (a) Blouin, N.; Leclerc, M. *Acc. Chem. Res.* **2008**, *41*, 1110−1119. (b) Yamamoto, T.; Takimiya, K. *J. Am. Chem. Soc.* **2007**, *129*, 2224−2225. (c) Takimiya, K.; Ebata, H.; Sakamoto, K.; Izawa, T.; Otsubo, T.; Kunugi, Y. *J. Am. Chem. Soc.* **2006**, *128*, 12604−12605.

(5) (a) Anthony, J. E.; Facchetti, A.; Heeney, M.; Marder, S. R.; Zhan, X. *Adv. Mater.* **2010**, *22*, 3876−3892. (b) Meng, Q.; Hu, W. *Phys. Chem. Chem. Phys.* **2012**, *14*, 14152−14164.

(6) (a) Nishida, J.-i.; Deno, H.; Ichimura, S.; Nakagawa, T.; Yamashita, Y. *J. Mater. Chem.* **2012**, *22*, 4483−4490. (b) Ie, Y.; Nitani, M.; Karakawa, M.; Tada, H.; Aso, Y. *Adv. Funct. Mater.* **2010**, *20*, 907−913. (c) Letizia, J. A.; Cronin, S.; Ortiz, R. P.; Facchetti, A.; Ratner, M. A.; Marks, T. J. *Chem.—Eur. J.* **2010**, *16*, 1911−1928.

(7) (a) Usta, H.; Risko, C.; Wang, Z.; Huang, H.; Deliomeroglu, M. K.; Zhukhovitskiy, A.; Facchetti, A.; Marks, T. J. *J. Am. Chem. Soc.* **2009**, *131*, 5586−5608. (b) Andrew, T. L.; Cox, J. R.; Swager, T. M. *Org. Lett.* **2010**, *12*, 5302−5305. (c) Andrew, T. L.; Bulović, V. *ACS Nano* **2012**, *6*, 4671−4677. (d) Zhou, Y.; Ding, L.; Shi, K.; Dai, Y.-Z.; Ai, N.; Wang, J.; Pei, J. *Adv. Mater.* **2012**, *24*, 957−961.

(8) Youn, J.; Huang, P.-Y.; Huang, Y.-W.; Chen, M.-C.; Lin, Y.-J.; Huang, H.; Ortiz, R. P.; Stern, C.; Chung, M.-C.; Feng, C.-Y.; Chen, L.-H.; Facchetti, A.; Marks, T. J. *Adv. Funct. Mater.* **2012**, *22*, 48−60.

(9) Ando, S.; Murakami, R.; Nishida, J.-i.; Tada, H.; Inoue, Y.; Tokito, S.; Yamashita, Y. *J. Am. Chem. Soc.* **2005**, *127*, 14996−14997.

(10) (a) Oh, J. H.; Suraru, S. L.; Lee, W.-Y.; Könemann, M.; Höffken, H. W.; Röger, C.; Schmidt, R.; Chung, Y.; Chen, W.-C.; Würthner, F.; Bao, Z. *Adv. Funct. Mater.* **2010**, *20*, 2148−2156. (b) Schmidt, R.; Oh, J. H.; Sun, Y.-S.; Deppisch, M.; Krause, A.-M.; Radacki, K.; Braunschweig, H.; Könemann, M.; Erk, P.; Bao, Z.; Würthner, F. *J. Am. Chem. Soc.* **2009**, *131*, 6215−6228.

(11) (a) Jäkle, F. *Chem. Rev.* **2010**, *110*, 3985−4022. (b) Wade, C. R.; Broomsgrove, A. E. J.; Aldridge, S.; Gabbaï, F. P. *Chem. Rev.* **2010**, *110*, 3958−3984. (c) Hudson, Z. M.; Wang, S. *Acc. Chem. Res.* **2009**, *42*, 1584−1596. (d) Mercier, L. G.; Piers, W. E.; Parvez, M. *Angew. Chem., Int. Ed.* **2009**, *48*, 6108−6111. (e) Wakamiya, A.; Mori, K.; Yamaguchi, S. *Angew. Chem., Int. Ed.* **2007**, *46*, 4273−4276. (f) Elbing, M.; Bazan, G. C. *Angew. Chem., Int. Ed.* **2008**, *47*, 834−838. (g) Saito, S.; Matsuo, K.; Yamaguchi, S. *J. Am. Chem. Soc.* **2012**, *134*, 9130−9133. (h) Zhou, Z.; Wakamiya, A.; Kushida, T.; Yamaguchi, S. *J. Am. Chem. Soc.* **2012**, *134*, 4529−4532.

(12) (a) Yamaguchi, S.; Tamao, K. *J. Chem. Soc., Dalton Trans.* **1998**, 3693−3702. (b) Chen, J.; Cao, Y. *Macromol. Rapid Commun.* **2007**, *28*, 1714−1742. (c) Chu, T.-Y.; Lu, J.; Beaupré, S.; Zhang, Y.; Pouliot, J.-R.; Wakim, S.; Zhou, J.; Leclerc, M.; Li, Z.; Ding, J.; Tao, Y. *J. Am. Chem. Soc.* **2011**, *133*, 4250−4253. (d) Schroeder, B. C.; Huang, Z.; Ashraf, R. S.; Smith, J.; D'Angelo, P.; Watkins, S. E.; Anthopoulos, T. D.; Durrant, J. R.; McCulloch, I. *Adv. Funct. Mater.* **2012**, *22*, 1663−1670. (e) Hou, J.; Chen, H.-Y.; Zhang, S.; Li, G.; Yang, Y. *J. Am. Chem. Soc.* **2008**, *130*, 16144−16145. (f) Coffin, R. C.; Peet, J.; Rogers, J.; Bazan, G. C. *Nat. Chem.* **2009**, *1*, 657−661.

(13) (a) Baumgartner, T.; Réau, R. *Chem. Rev.* **2006**, *106*, 4681−4727; Correction: **2007**, *107*, 303. (b) Crassous, J.; Réau, R. *Dalton Trans.* **2008**, 6865−6876. (c) Matano, Y.; Imahori, H. *Org. Biomol. Chem.* **2009**, *7*, 1258−1271. (d) Ren, Y.; Baumgartner, T. *Dalton Trans.* **2012**, *41*, 7792−7800.

(14) (a) Baumgartner, T.; Neumann, T.; Wirges, B. *Angew. Chem., Int. Ed.* **2004**, *43*, 6197−6201. (b) Baumgartner, T.; Bergmans, W.; Kárpáti, T.; Neumann, T.; Nieger, M.; Nyulászi, L. *Chem.—Eur. J.* **2005**, *11*, 4687−4699. (c) Dienes, Y.; Durben, S.; Kárpáti, T.; Neumann, T.; Englert, U.; Nyulászi, L.; Baumgartner, T. *Chem.—Eur. J.* **2007**, *13*, 7487−7500. (d) Romero-Nieto, C.; Durben, S.; Kormos, I. M.; Baumgartner, T. *Adv. Funct. Mater.* **2009**, *19*, 3625−3631. (e) Ren, Y.; Baumgartner, T. *J. Am. Chem. Soc.* **2011**, *133*, 1328−1340. (f) Ren, Y.; Kan, W. H.; Henderson, M. A.; Bomben, P. G.; Berlinguette, C. P.; Thangadurai, V.; Baumgartner, T. *J. Am. Chem. Soc.* **2011**, *133*, 17014−17026. (g) Ren, Y.; Kan, W. H.; Thangadurai, V.; Baumgartner, T. *Angew. Chem., Int. Ed.* **2012**, *51*, 3964−3968. (h) Durben, S.; Baumgartner, T. *Angew. Chem., Int. Ed.* **2011**, *50*, 7948−7952. (i) Durben, S.; Baumgartner, T. *Inorg. Chem.* **2011**, *50*, 6823−6836.

(15) (a) Bouit, P. A.; Escande, A.; Szűcs, R.; Szieberth, D.; Lescop, C.; Nyulászi, L.; Hissler, M.; Réau, R. *J. Am. Chem. Soc.* **2012**, *134*, 6524−6527. (b) Joly, D.; Tondelier, D.; Deborde, V.; Delaunay, W.; Thomas, A.; Bhanuprakash, K.; Geffroy, B.; Hissler, M.; Réau, R. *Adv. Funct. Mater.* **2012**, *22*, 567−576. (c) Fadhel, O.; Gras, M.; Lemaitre, N.; Deborde, V.; Hissler, M.; Geffroy, B.; Réau, R. *Adv. Mater.* **2009**, *21*, 1261−1265. (d) Su, H.-C.; Fadhel, O.; Yang, C.-J.; Cho, T.-Y.; Fave, C.; Hissler, M.; Wu, C.-C.; Réau, R. *J. Am. Chem. Soc.* **2006**, *128*, 983−995. (e) Fave, C.; Cho, T.-Y.; Hissler, M.; Chen, C.-W.; Luh, T.-Y.; Wu, C.-C.; Réau, R. *J. Am. Chem. Soc.* **2003**, *125*, 9254−9255.

(16) (a) Bruch, A.; Fukazawa, A.; Yamaguchi, E.; Yamaguchi, S.; Studer, A. *Angew. Chem., Int. Ed.* **2011**, *50*, 12094−12098. (b) Tsurusaki, A.; Sasamori, T.; Wakamiya, A.; Yamaguchi, S.; Nagura, K.; Irle, S.; Tokitoh, N. *Angew. Chem., Int. Ed.* **2011**, *50*, 10940−10943. (c) Fukazawa, A.; Yamaguchi, E.; Ito, E.; Yamada, H.; Wang, J.; Irle, S.; Yamaguchi, S. *Organometallics* **2011**, *30*, 3870−3879. (d) Fukazawa, A.; Hara, M.; Okamoto, T.; Son, E.-C.; Xu, C.; Tamao, K.; Yamaguchi, S. *Org. Lett.* **2008**, *10*, 913−916.

(17) (a) Matano, Y.; Saito, A.; Fukushima, T.; Tokudome, Y.; Suzuki, F.; Sakamaki, D.; Kaji, H.; Ito, A.; Tanaka, K.; Imahori, H. *Angew. Chem., Int. Ed.* **2011**, *50*, 8016−8020. (b) Saito, A.; Miyajima, T.; Nakashima, M.; Fukushima, T.; Kaji, H.; Matano, Y.; Imahori, H. *Chem.—Eur. J.* **2009**, *15*, 10000−10004. (c) Nakabuchi, T.;

Nakashima, M.; Fujishige, S.; Nakano, H.; Matano, Y.; Imahori, H. *J. Org. Chem.* **2010**, *75*, 375−389. (d) Matano, Y.; Saito, A.; Suzuki, Y.; Miyajima, T.; Akiyama, S.; Otsubo, S.; Nakamoto, E.; Aramaki, S.; Imahori, H. *Chem.—Asian J.* **2012**, *7*, 2305−2312.
(18) (a) Tsuji, H.; Sato, K.; Sato, Y.; Nakamura, E. *J. Mater. Chem.* **2009**, *19*, 3364−3366. (b) Tsuji, H.; Sato, K.; Sato, Y.; Nakamura, E. *Chem.—Asian J.* **2010**, *5*, 1294−1297. (c) Nakano, K.; Oyama, H.; Nishimura, Y.; Nakasako, S.; Nozaki, K. *Angew. Chem., Int. Ed.* **2012**, *51*, 695−699.
(19) (a) Letizia, J. A.; Salata, M. R.; Tribout, C. M.; Facchetti, A.; Ratner, M. A.; Marks, T. J. *J. Am. Chem. Soc.* **2008**, *130*, 9679−9694. (b) Guo, X.; Ortiz, R. P.; Zheng, Y.; Hu, Y.; Noh, Y.-Y.; Baeg, K.-J.; Facchetti, A.; Marks, T. J. *J. Am. Chem. Soc.* **2011**, *133*, 1405−1418. (c) Zhou, N.; Guo, X.; Ortiz, R. P.; Li, S.; Zhang, S.; Chang, R. P. H.; Facchetti, A.; Marks, T. J. *Adv. Mater.* **2012**, *24*, 2242−2248. (d) Guo, X.; Zhou, N.; Lou, S. J.; Hennek, J. W.; Ortiz, R. P.; Butler, M. R.; Boudreault, P.-L. T.; Strzalka, J.; Morin, P.-O.; Leclerc, M.; Navarrete, J. T. L.; Ratner, M. A.; Chen, L. X.; Chang, R. P. H.; Facchetti, A.; Marks, T. J. *J. Am. Chem. Soc.* **2012**, *134*, 18427−18439.
(20) (a) Barron, A. R.; Hall, S. W.; Cowley, A. H. *J. Chem. Soc., Chem. Commun.* **1987**, 1753−1754. (b) Decken, A.; Gill, E. D.; Bottomley, F. *Acta Crystallogr.* **2004**, *E60*, o1456−o1457. (c) Saunders, A. J.; Crossley, I. R.; Coles, M. P.; Roe, S. M. *Chem. Commun.* **2012**, *48*, 5766−5768.
(21) Uhlig, W.; Tzschach, A. *Z. Anorg. Allg. Chem.* **1989**, *576*, 281−283.
(22) Meldal, M.; Tornøe, C. W. *Chem. Rev.* **2008**, *108*, 2952−3015.
(23) (a) Lal, S.; Díez-González, S. *J. Org. Chem.* **2011**, *76*, 2367−2373. (b) Pérez-Balderas, F.; Ortega-Muñoz, M.; Morales-Sanfrutos, J.; Hernández-Mateo, F.; Calvo-Flores, F. G.; Calvo-Asín, J. A.; Isac-García, J.; Santoyo-González, F. *Org. Lett.* **2003**, *5*, 1951−1954.
(24) Garrou, P. E. *Chem. Rev.* **1981**, *81*, 229−266.
(25) Wright, V. A.; Patrick, B. O.; Schneider, C.; Gates, D. P. *J. Am. Chem. Soc.* **2006**, *128*, 8836−8844.
(26) (a) Yao, S.; Ahn, H.-Y.; Wang, X.; Fu, J.; Van Stryland, E. W.; Hagan, D. J.; Belfield, K. D. *J. Org. Chem.* **2010**, *75*, 3965−3974. (b) Ellinger, S.; Graham, K. R.; Shi, P.; Farley, R. T.; Steckler, T. T.; Brookins, R. N.; Taranekar, P.; Mei, J.; Padilha, L. A.; Ensley, T. R.; Hu, H.; Webster, S.; Hagan, D. J.; Van Stryland, E. W.; Schanze, K. S.; Reynolds, J. R. *Chem. Mater.* **2011**, *23*, 3805−3817.
(27) (a) Wu, H.; Ying, L.; Yang, W.; Cao, Y. *Chem. Soc. Rev.* **2009**, *38*, 3391−3400. (b) Park, S.; Kwon, J. E.; Kim, S. H.; Seo, J.; Chung, K.; Park, S.-Y.; Jang, D.-J.; Medina, B. M.; Gierschner, J.; Park, S. Y. *J. Am. Chem. Soc.* **2009**, *131*, 14043−14049. (c) Tang, K.-C.; Chang, M.-J.; Lin, T.-Y.; Pan, H.-A.; Fang, T.-C.; Chen, K.-Y.; Hung, W.-Y.; Hsu, Y.-H.; Chou, P.-T. *J. Am. Chem. Soc.* **2011**, *133*, 17738−17745.
(28) (a) Valeur, B. *Molecular Fluorescence: Principles and Applications*; Wiley-VCH: Weinheim, Germany, 2002. (b) Grabowski, Z. R.; Rotkiewicz, K.; Rettig, W. *Chem. Rev.* **2003**, *103*, 3899.
(29) Lu, B.-Y.; Li, Z.-M.; Zhu, Y.-Y.; Zhao, X.; Li, Z.-T. *Tetrahedron* **2012**, *68*, 8857−8862.
(30) (a) Yam, V. W. W.; Cheng, E. C. C. *Top. Curr. Chem.* **2007**, *281*, 206−309. (b) Dienes, Y.; Eggenstein, M.; Neumann, T.; Englert, U.; Baumgartner, T. *Dalton Trans.* **2006**, 1424−1433.
(31) Pommerehne, J.; Vestweber, H.; Guss, W.; Mahrt, R. F.; Bässler, H.; Porsch, M.; Daub, J. *Adv. Mater.* **1995**, *7*, 551−554.
(32) Brabec, C. J.; Sariciftci, N. S.; Hummelen, J. C. *Adv. Funct. Mater.* **2001**, *11*, 15−26.
(33) Frisch, M. J.; et al. *Gaussian 09*, revision A.02; Gaussian, Inc.: Wallingford, CT, 2009.
(34) The energy levels of **BTI** were calculated with Gaussian 03, revision E.1, at the B3LYP/6-31G(d) level of theory.
(35) The X-ray data for **1** were used as input for the TD-DFT calculation.
(36) (a) Ajayaghosh, A.; Praveen, V. K.; Vijayakumar, C. *Chem. Soc. Rev.* **2008**, *37*, 109−122. (b) Ajayaghosh, A.; Vijayakumar, C.; Praveen, V. K.; Babu, S. S.; Varghese, P. *J. Am. Chem. Soc.* **2006**, *128*, 7174−7175. (c) Praveen, V. K.; George, S. J.; Varghese, R.; Vijayakumar, C.; Ajayaghosh, A. *J. Am. Chem. Soc.* **2006**, *128*, 7542−7550. (d) Ajayaghosh, A.; George, S. J.; Praveen, V. K. *Angew. Chem., Int. Ed.* **2003**, *42*, 481−484. (e) Yang, X.; Zhang, G.; Zhang, D. *J. Mater. Chem.* **2012**, *22*, 38−50. (f) Steed, J. W. *Chem. Commun.* **2011**, *47*, 1379−1383. (g) Romero-Nieto, C.; Marcos, M.; Merino, S.; Barberá, J.; Baumgartner, T.; Rodríguez-López, J. *Adv. Funct. Mater.* **2011**, *21*, 4088−4099.